ELectronics EXpress

LETTER

IEICE Electronics Express, Vol.13, No.3, 1–9

Time-domain asymptotic-numerical solution for transient scattered field from a cylindrically curved conducting open sheet excited by UWB pulse wave

Keiji Goto[a)], **Naoki Kishimoto, and Oki Okawa**

Department of Communications Engineering, National Defense Academy, 1–10–20 Hashirimizu, Yokosuka, Kanagawa 239–8686, Japan

a) *keigoto@nda.ac.jp*

Abstract: A time-domain (TD) asymptotic-numerical solution (TD-ANS) for a transient scattered field, which is a useful new reference solution on engineering applications, is developed for a two-dimensional transient scattered field from a cylindrically curved conducting open sheet excited by an ultra-wideband (UWB) pulse wave. The TD-ANS is represented by a combination of pulse wave elements; each element is obtained from a numerical integration. The TD-ANS is highly accurate and is useful in understanding transient scattering phenomena. The computation rate of the TD-ANS is very fast compared with that of a reference solution. The validity and usefulness of the proposed TD-ANS are confirmed by comparing with a reference solution and experimental-numerical results.

Keywords: time-domain, asymptotic-numerical solution, transient scattered field, cylindrically curved conducting open sheet, UWB pulse wave

Classification: Electromagnetic theory

References

[1] P. R. Rousseau and P. H. Pathak: IEEE Trans. Antennas Propag. **43** (1995) 1375. DOI:10.1109/8.475925

[2] F. A. Molinet: IEEE Antennas Propag. Mag. **47** (2005) 34. DOI:10.1109/MAP.2005.1599164

[3] K. Goto, T. Kawano and T. Ishihara: IEICE Trans. Electron. **E92-C** (2009) 25. DOI:10.1587/transele.E92.C.25

[4] M. Albani, G. Carluccio and P. H. Pathak: IEEE Trans. Antennas Propag. **63** (2015) 3136. DOI:10.1109/TAP.2015.2427877

[5] K. Goto, M. Sawada, K. Mori and Y. Horii: IEICE Electron. Express **11** (2014) 20130963. DOI:10.1587/elex.11.20130963

[6] K. Goto, T. Kawano and T. Ishihara: IEICE Electron. Express **8** (2011) 561. DOI:10.1587/elex.8.561

[7] Federal Communications Commission (FCC): First report and order: Revision of part 15 of the commission's rules regarding ultra-wideband transmission

DOI: 10.1587/elex.13.20151041
Received December 7, 2015
Accepted December 28, 2015
Publicized January 18, 2016
Copyedited February 10, 2016

systems, FCC 02-08, Washington, D.C., 22 April 2002.
[8] K. Goto, O. Okawa and N. Kishimoto: The Papers of Technical Meeting on Electromagnetic Theory, IEE Japan, EMT-15-70 (2015) 37.
[9] K. Goto, N. Sumikawa, T. Santikul and R. Asai: ICEAA (2015) 227. DOI: 10.1109/ICEAA.2015.7297109
[10] E. O. Brigham: *The Fast FourierTtransform* (Prentice-Hall, New Jersey, 1974).
[11] A. Michaeli: IEEE Trans. Antennas Propag. **37** (1989) 1073. DOI:10.1109/8.35785
[12] K. Goto, T. Ajiki, T. Kawano and T. Ishihara: ISAP (2006) 2D2b2.
[13] P. H. Pathak: Radio Sci. **14** (1979) 419. DOI:10.1029/RS014i003p00419
[14] L. B. Felsen: *Transient Electromagnetic Fields* (Springer-Verlag, New York, 1976).
[15] M. Abramowitz and I. A. Stegun: *Handbook of mathematical Functions* (Dover, New York, 1972).
[16] W. A. Johnson and R. W. Ziolkowski: Radio Sci. **19** (1984) 275. DOI:10.1029/RS019i001p00275

1 Introduction

Analytical and numerical studies on the frequency-domain (FD) and time-domain (TD) scattered fields by smooth curved structures with edges or wedges have been conducted on the application area such as the radar cross section, high resolution radar, and target identification [1, 2, 3, 4].

We have derived a TD asymptotic solution [5] for a two-dimensional (2-D) transient scattered field excited by the edges of a cylindrically curved conducting open sheet by applying the Fourier transform method. However, The TD asymptotic solution in [5] has a limitation on engineering applications, because it becomes increasingly inaccurate as the fractional bandwidth (FB) of an incident pulse wave increases gradually [6].

In this paper, in order to overcome the limitation of the TD asymptotic solution [5], we develop a TD asymptotic-numerical solution (TD-ANS) for a 2-D transient scattered field when an ultra-wideband (UWB) pulse wave [7] is incident on a cylindrically curved conducting open sheet [8, 9]. The TD-ANS is represented by a combination of pulse wave elements; each element is obtained numerically by applying the fast Fourier transform (FFT) numerical code [10] to a pulse wave element integral. The TD-ANS is highly accurate and can extract and observe each pulse wave element from a response waveform. Furthermore, the computation rate of the TD-ANS is very fast compared with that of a reference solution.

The validity and usefulness of the TD-ANS presented here are confirmed by comparing with the reference solution and experimental-numerical results. The time convention $\exp(-i\omega t)$ is adopted and suppressed in this paper.

2 Time-domain asymptotic-numerical solution (TD-ANS)

2.1 Formulation and frequency-domain uniform asymptotic solution (FD-UAS)

Fig. 1(a) shows a 2-D cylindrically curved conducting open sheet with two straight edges A and B (to be called a curved open sheet) defined by $\rho = a$, $0 \leq \phi \leq \phi_{AB}$,

DOI: 10.1587/elex.13.20151041
Received December 7, 2015
Accepted December 28, 2015
Publicized January 18, 2016
Copyedited February 10, 2016

$-\infty < z < +\infty$, and coordinate systems (x, y, z), (ρ, ϕ), and (r, ψ). We assume that the radius of curvature $\rho = a$ is sufficiently large compared with the wavelength (i.e., $\omega a/c \gg 1$, ω: angular frequency, c: speed of light) and that a high-frequency (HF) plane wave which has only a magnetic field component in the z-axis propagates along the positive x-direction.

The z-component of the FD scattered field $u(\boldsymbol{r}, \omega)$ ($\equiv u(\omega)$, hereafter the position vector $\boldsymbol{r} = (r, \psi)$ is dropped in the notations) from a curved open sheet is represented approximately by a FD uniform asymptotic solution (FD-UAS) as follows

$$u(\omega) \sim u_{\text{FD-UAS}}(\omega) = u_{\text{A,FD-UAS}}(\omega) + u_{\text{B,FD-UAS}}(\omega) + u_{\text{FD-RGO}}(\omega). \tag{1}$$

Here, $u_{\text{A,FD-UAS}}(\omega)$, $u_{\text{B,FD-UAS}}(\omega)$, and $u_{\text{FD-RGO}}(\omega)$, which are components of the $u_{\text{FD-UAS}}(\omega)$, denote the FD-UAS for the scattered field excited by the edge A, the FD-UAS for the scattered field excited by the edge B, and the analytical solution of a reflected geometric optical ray (RGO) reflected on the convex surface of a curved open sheet, respectively. Readers may find explicit representations and propagation paths of $u_{\text{A,FD-UAS}}(\omega)$ and $u_{\text{FD-RGO}}(\omega)$ in [3, 5, 11, 12, 13].

The $u_{\text{B,FD-UAS}}(\omega)$ in (1) is given by

$$u_{\text{B,FD-UAS}}(\omega) = \exp(i\omega L_{\text{Q}_{0\text{B}}\text{B}}/c) \sum_j \left[\sum_r^{R_{\text{B}}} U_{\text{B},j}(\text{P}) u_{\text{B},j}(\omega) \right]$$

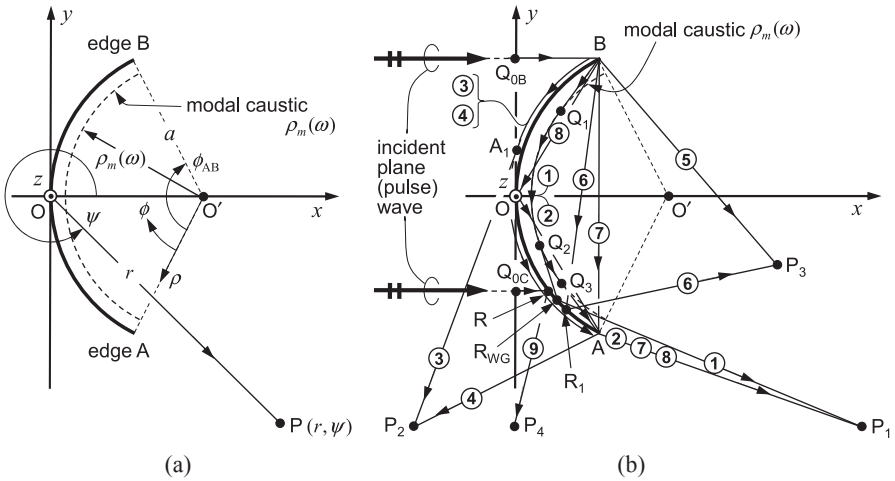

Fig. 1. Scattering phenomena of scattered field excited by the edge B of a curved open sheet. (a) Curved open sheet (a, ϕ_{AB}) and coordinate systems (x, y, z), (ρ, ϕ), and (r, ψ). (b) Propagation paths of scattered field elements excited by the edge B and the propagation path of RGO reflected on a convex surface. ①: $\text{Q}_{0\text{B}} \to \text{B} \to \text{Q}_1 \curvearrowright \text{Q}_2 \to \text{R}_{\text{WG}} \to \text{P}_1$, ②: $\text{Q}_{0\text{B}} \to \text{B} \to \text{Q}_1 \curvearrowright \text{Q}_3 \to \text{A} \to \text{P}_1$, ③: $\text{Q}_{0\text{B}} \to \text{B} \curvearrowright \text{A}_1 \to \text{P}_2$, ④: $\text{Q}_{0\text{B}} \to \text{B} \curvearrowright \text{A} \to \text{P}_2$, ⑤: $\text{Q}_{0\text{B}} \to \text{B} \to \text{P}_3$, ⑥: $\text{Q}_{0\text{B}} \to \text{B} \to \text{R}_1 \to \text{P}_3$, ⑦: $\text{Q}_{0\text{B}} \to \text{B} \to \text{A} \to \text{P}_1$, ⑧: $\text{Q}_{0\text{B}} \to \text{B} \to \text{O} \to \text{A} \to \text{P}_1$, ⑨: $\text{Q}_{0\text{C}} \to \text{R} \to \text{P}_4$. Here, notation $\text{Q}_1 \curvearrowright \text{Q}_2(\text{Q}_3)$ denotes the propagation path along the modal caustic $\rho_m(\omega)$ from the point Q_1 to the point $\text{Q}_2(\text{Q}_3)$. While, notation $\text{B} \curvearrowright \text{A}_1(\text{A})$ is the propagation path along the convex surface $(\rho = a)$ from the edge B to the point A_1 (the edge A).

DOI: 10.1587/elex.13.20151041
Received December 7, 2015
Accepted December 28, 2015
Publicized January 18, 2016
Copyedited February 10, 2016

$$\text{where } (j, r, R_{\mathrm{B}}) = (\mathrm{WG}_m, m = 1, M_{\mathrm{B}}), (\mathrm{SD}_n, n = 1, N_{\mathrm{B},1}), \quad (2)$$
$$(\mathrm{CW}_n\mathrm{ED}, n = 1, N_{\mathrm{B},2}), (\mathrm{RGO}_k, k = 0, K_{\mathrm{B},1}),$$
$$(\mathrm{RED}_k, k = 0, K_{\mathrm{B},2}).$$

The scattering phenomena of $u_{\mathrm{B,FD\text{-}UAS}}(\omega)$ are depicted in Fig. 1(b). In (2), $L_{\mathrm{Q_{0B}B}}$ is the distance of an incident plane wave along the straight-line path $\mathrm{Q_{0B}} \rightarrow \mathrm{B}$ which propagates from the reference point $\mathrm{Q_{0B}}$ on the y-axis to the edge B. Notations $u_{\mathrm{B,WG}_m}(\omega)$, $u_{\mathrm{B,SD}_n}(\omega)$, $u_{\mathrm{B,CW}_n\mathrm{ED}}(\omega)$, $u_{\mathrm{B,RGO}_k}(\omega)$, and $u_{\mathrm{B,RED}_k}(\omega)$ are the FD scattered filed elements of the $u_{\mathrm{B,FD\text{-}UAS}}(\omega)$ and denote respective the mth-order whispering-gallery mode radiation field (WG_m) (① and ②: $m = M_{\mathrm{B}} = 1$, see [3, 6]), the nth-order surface diffracted ray (SD_n) (③: $n = N_{\mathrm{B},1} = 1$), the nth-order creeping wave incidence and edge diffracted ray ($\mathrm{CW}_n\mathrm{ED}$) (④: $n = N_{\mathrm{B},2} = 1$), the k times RGO (RGO_k) (⑤: $k = 0$ and ⑥: $k = K_{\mathrm{B},1} = 1$), and the k times reflected and edge diffracted ray (RED_k) (⑦: $k = 0$ and ⑧: $k = K_{\mathrm{B},2} = 1$). The notation $U_{\mathrm{B},j}(\mathrm{P})$ is a unit step function and is defined as $U_{\mathrm{B},j}(\mathrm{P}) = 1$ (or $U_{\mathrm{B},j}(\mathrm{P}) = 0$) when the FD scattered field element $u_{\mathrm{B},j}(\omega)$ can (or cannot) reach the observation point P.

2.2 Transient scattered field integral

The transient scattered field $y(\boldsymbol{r}, t)(\equiv y(t))$ from a curved open sheet can be expressed by the inverse Fourier transform of the product of the FD scattered field $u(\omega)$ and the frequency spectrum $S(\omega)$ of a pulse source function $s(t)$ [14].

$$y(t) = \frac{1}{2\pi}\int_{-\infty}^{\infty} u(\omega)S(\omega)\exp(-i\omega t)d\omega. \quad (3)$$

We assume a truncated Gaussian-type modulated pulse source $s(t)$:

$$s(t) = \begin{cases} \exp[-i\omega_0(t - t_0) - (t - t_0)^2/(2d)^2] & \text{for} \quad 0 \le t \le 2t_0 \\ 0 & \text{for} \quad t < 0, t > 2t_0 \end{cases} \quad (4)$$

where ω_0 denotes a central angular frequency, and t_0 and d are constant parameters. The frequency spectrum $S(\omega)$ of the $s(t)$ in (4) is given by

$$S(\omega) = 2d\sqrt{\pi}\,\mathrm{Re}[\mathrm{erf}\,\beta(\omega)]\exp[i\omega t_0 - d^2(\omega - \omega_0)^2] \quad (5)$$

$$\beta(\omega) = \frac{t_0}{2d} - id(\omega - \omega_0) \quad (6)$$

where $\mathrm{erf}\,z$ is the error function [15] defined by

$$\mathrm{erf}\,z = \frac{2}{\sqrt{\pi}}\int_0^z \exp(-t^2)dt. \quad (7)$$

Figs. 2(a) and 2(b) illustrate the real part of the $s(t)$ in (4) and the absolute value of the $S(\omega)$ in (5), respectively. Numerical parameters used in the calculations are given in the caption of Fig. 2. The main portion of the $S(\omega)$ is distributed within the HF region ($\omega_{\mathrm{L}} \le \omega \le \omega_{\mathrm{H}}$). For these numerical parameters, the $s(t)$ in (4) becomes a Gaussian-type modulated UWB pulse source, because the FB of $S(\omega)$ is 0.277 and satisfies the condition of UWB (FB $\ge$ 0.25) in [7].

After substituting the numerical solution for the FD scattered field $u(\omega)$ computed from the method of moment (MoM) [16] and the $S(\omega)$ in (5) into the

DOI: 10.1587/elex.13.20151041
Received December 7, 2015
Accepted December 28, 2015
Publicized January 18, 2016
Copyedited February 10, 2016

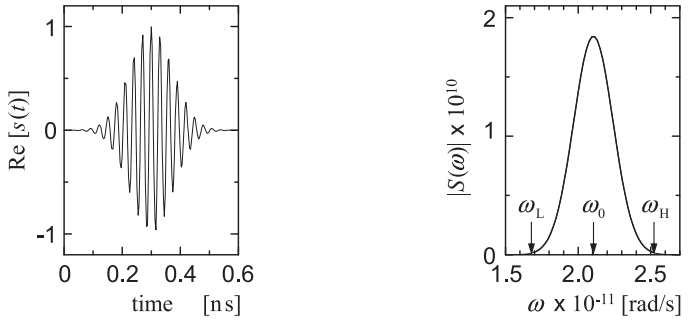

(a) Real part of $s(t)$. (b) Absolute value of $S(\omega)$.

Fig. 2. Gaussian-type modulated UWB pulse source $s(t)$ defined by (4). Numerical parameters: $\omega_0 = 2.105 \times 10^{11}$ rad/s, $t_0 = 3.0 \times 10^{-10}$ s, $d = 5.20 \times 10^{-11}$ s. Where $\omega_L = 1.696 \times 10^{11}$ rad/s, $\omega_H = 2.513 \times 10^{11}$ rad/s, and FB = 0.277.

integral $y(t)$ in (3), by applying the FFT numerical code [10] to the integral $y(t)$, one obtains the reference solution $y_{\text{reference}}(t)$ numerically. Moreover, replacing the integrand $u(\omega)S(\omega)$ in (3) with the experimental data for the FD scattered field $u(\omega)$ measured using a bistatic experiment device in an anechoic chamber and the $S(\omega)$ in (5) and then applying the FFT numerical code [10] to the $y(t)$ in (3) yield the experimental-numerical results $y_{\text{exp-num}}(t)$.

The response waveform of $y(t)$ in (3) is obtained from the real part of $y(t)$, namely, Re$[y(t)]$. In section 3, the response waveforms Re$[y_{\text{reference}}(t)]$ and Re$[y_{\text{exp-num}}(t)]$ are used to confirm the validity and usefulness of the TD-ANS derived in Section 2.3.

2.3 TD-ANS for the transient scattered field

By substituting the $u_{\text{FD-UAS}}(\omega)$ in (1) into (3), we obtain the following representation:

$$y(t) \sim y_{\text{A}}(t) + y_{\text{B}}(t) + y_{\text{RGO}}(t) \tag{8}$$

where $y_{\text{A}}(t)$, $y_{\text{B}}(t)$, and $y_{\text{RGO}}(t)$, which are components of the $y(t)$, denote the transient scattered field excited by the edge A, the transient scattered field excited by the edge B, and the transient RGO, respectively.

The transient scattered field component $y_{\text{B}}(t)$ in (8) is represented by

$$y_{\text{B}}(t) = \sum_j \left[\sum_r^{R_{\text{B}}} U_{\text{B},j}(\text{P}) y_{\text{B},j}(t) \right]. \tag{9}$$

In (9), $y_{\text{B},j}(t)$, $j = \text{WG}_m$, SD_n, CW_nED, RGO_k, and RED_k, denotes a pulse wave element and is given by the following inverse Fourier transform of the product of the FD scattered field element $\exp(i\omega L_{Q_{0\text{B}}\text{B}}/c)u_{\text{B},j}(\omega)$ in (2) and the frequency spectrum $S(\omega)$ in (5).

$$y_{\text{B},j}(t) = \frac{1}{2\pi} \int_{-\infty}^{\infty} \exp(i\omega L_{Q_{0\text{B}}\text{B}}/c) u_{\text{B},j}(\omega) S(\omega) \exp(-i\omega t) d\omega. \tag{10}$$

The pulse wave element $y_{\text{B},j}(t)$ represented by the integral form in (10) is calculable numerically by applying the FFT numerical code [10]. By substituting

DOI: 10.1587/elex.13.20151041
Received December 7, 2015
Accepted December 28, 2015
Publicized January 18, 2016
Copyedited February 10, 2016

the numerical solution $y_{B,j}(t)$ in (10) into the $y_B(t)$ in (9), we derive the TD-ANS for the $y_B(t)$ as follows

$$y_{B,\text{TD-ANS}}(t) = \sum_j \left[\sum_r^{R_B} U_{B,j}(\text{P}) y_{B,j}(t) \right]. \tag{11}$$

The TD-ANSs for $y_A(t)$ and $y_{RGO}(t)$ in (8), namely, the $y_{A,\text{TD-ANS}}(t)$ and the $y_{\text{TD-RGO}}(t)$ can be analogized easily from the above-mentioned analytical-numerical method and are represented by

$$y_{A,\text{TD-ANS}}(t) = \sum_j \left[\sum_r^{R_A} U_{A,j}(\text{P}) y_{A,j}(t) \right]$$

$$\begin{aligned} \text{where } (j, r, R_A) = {} & (\text{WG}_m, m = 1, M_A), (\text{SD}_n, n = 1, N_{A,1}), \\ & (\text{CW}_n\text{ED}, n = 1, N_{A,2}), (\text{RGO}_k, k = 0, K_{A,1}), \\ & (\text{RED}_k, k = 0, K_{A,2}). \end{aligned} \tag{12}$$

$$y_{A,j}(t) = \frac{1}{2\pi} \int_{-\infty}^{\infty} \exp(i\omega L_{Q_{0A}A}/c) u_{A,j}(\omega) S(\omega) \exp(-i\omega t) d\omega \tag{13}$$

$$y_{\text{TD-RGO}}(t) = \frac{1}{2\pi} \int_{-\infty}^{\infty} U_{\text{RGO}}(\text{P}) \exp(i\omega L_{Q_{0C}R}/c) u_{\text{FD-RGO}}(\omega) S(\omega) \exp(-i\omega t) d\omega \tag{14}$$

where $L_{Q_{0A}A}$ ($L_{Q_{0C}R}$) is the distance of an incident plane pulse wave along the straight-line path $Q_{0A} \rightarrow A$ ($Q_{0C} \rightarrow R$) which propagates from the reference point Q_{0A} (Q_{0C}) on the y-axis to the edge A (the reflection point R (see Fig. 1(b))). The unit step function $U_{A,j}(\text{P})$($U_{\text{RGO}}(\text{P})$) stands for 1 when the $y_{A,j}(t)$ (the RGO) can reach the observation point P, and for 0 when the $y_{A,j}(t)$ (the RGO) cannot reach the point P.

By substituting $y_{A,\text{TD-ANS}}(t)$ in (12), $y_{B,\text{TD-ANS}}(t)$ in (11), and $y_{\text{TD-RGO}}(t)$ in (14) into $y_A(t)$, $y_B(t)$, and $y_{RGO}(t)$ in (8), we develop the TD-ANS for the transient scattered field $y(t)$ as follows

$$\begin{aligned} y_{\text{TD-ANS}}(t) &= y_{A,\text{TD-ANS}}(t) + y_{B,\text{TD-ANS}}(t) + y_{\text{TD-RGO}}(t) \\ &= \sum_j \left[\sum_r^{R_A} U_{A,j}(\text{P}) y_{A,j}(t) \right] + \sum_j \left[\sum_r^{R_B} U_{B,j}(\text{P}) y_{B,j}(t) \right] + y_{\text{TD-RGO}}(t). \end{aligned} \tag{15}$$

The TD-ANS in (15) is represented by a combination of pulse wave elements $y_{A,j}(t)$, $y_{B,j}(t)$, and $y_{\text{TD-RGO}}$. Therefore, the response waveform Re[$y_{\text{TD-ANS}}(t)$] can extract and observe each pulse wave element from the Re[$y(t)$].

3 Numerical results and discussions

In this section, we perform numerical calculations and measurement experimentations required to assess the validity and usefulness of the TD-ANS derived in Section 2.3 when a UWB pulse wave is incident on a curved open sheet.

First, we investigate the accuracy and computation rate of the TD-ANS. Figs. 3(a) and 3(b) show the response waveform vs. time curves observed at the observation point P(r, ψ) (see Fig. 1(a)). Numerical parameters used in the calcu-

DOI: 10.1587/elex.13.20151041
Received December 7, 2015
Accepted December 28, 2015
Publicized January 18, 2016
Copyedited February 10, 2016

lations are given in the caption of Fig. 3 and the time t is set $t = 0$ when the Gaussian-type modulated UWB plane pulse wave traverses the y-axis (see Fig. 1(b)). The response waveform $\mathrm{Re}[y_{\text{TD-ANS}}(t)]$ (—: solid curve) given by

$$\mathrm{Re}[y_{\text{TD-ANS}}(t)] = \mathrm{Re}[y_{\text{A,TD-ANS}}(t)] + \mathrm{Re}[y_{\text{B,TD-ANS}}(t)] + \mathrm{Re}[y_{\text{TD-RGO}}(t)] \quad (16)$$

where

$$\mathrm{Re}[y_{\text{A,TD-ANS}}(t)] = \mathrm{Re}[y_{\text{A,WG}_1}(t)] + \mathrm{Re}[y_{\text{A,CW}_1\text{ED}}(t)] + \mathrm{Re}[y_{\text{A,RGO}_0}(t)] + \mathrm{Re}[y_{\text{A,RED}_0}(t)] + \mathrm{Re}[y_{\text{A,RED}_1}(t)] \quad (17)$$

$$\mathrm{Re}[y_{\text{B,TD-ANS}}(t)] = \mathrm{Re}[y_{\text{B,WG}_1}(t)] + \mathrm{Re}[y_{\text{B,SD}_1}(t)] + \mathrm{Re}[y_{\text{B,CW}_1\text{ED}}(t)] + \mathrm{Re}[y_{\text{B,RGO}_0}(t)] + \mathrm{Re}[y_{\text{B,RED}_0}(t)] + \mathrm{Re}[y_{\text{B,RED}_1}(t)] \quad (18)$$

agrees excellently with the response waveform $\mathrm{Re}[y_{\text{reference}}(t)]$ (---: red dashed curve) calculated from the reference solution (see Section 2.2 and Fig. 3(a)) and the

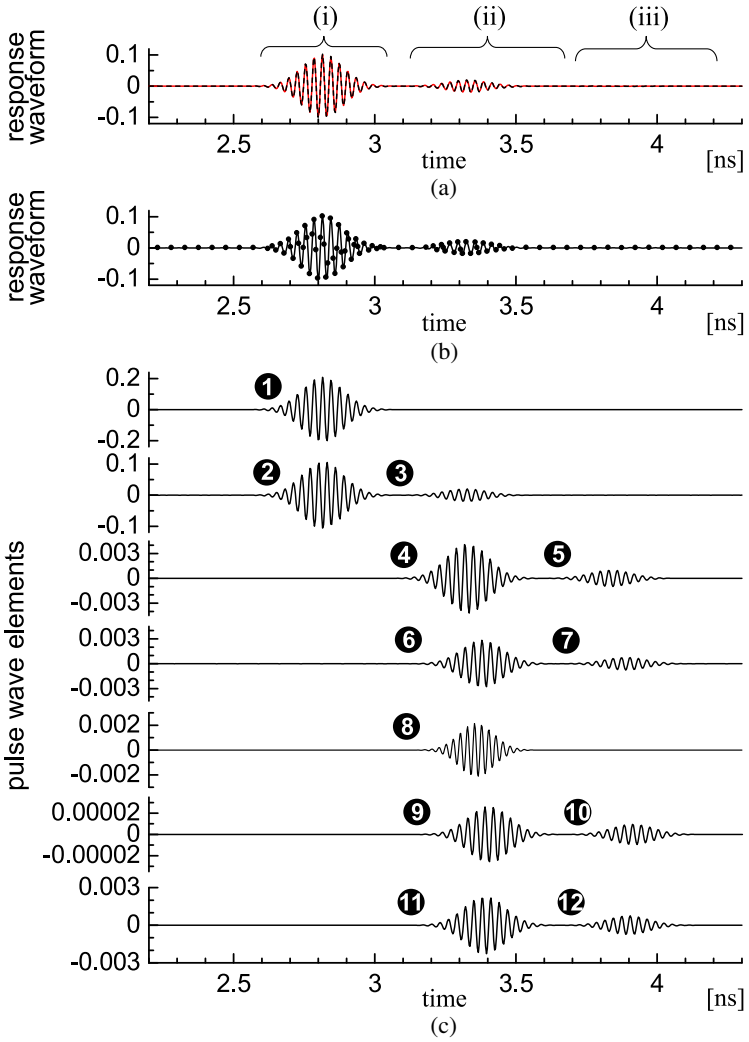

Fig. 3. Response waveform (Figs. 3(a) and 3(b)) and pulse wave elements (Fig. 3(c)) from a curved open sheet excited by UWB plane pulse wave. Numerical parameters: curved open sheet $(a, \phi_{\text{AB}}) = (1.01 \times 10^{-1}\,\text{m}, 99.6°)$ and observation point $\text{P}(r, \psi) = (0.8\,\text{m}, 280°)$. UWB pulse source $s(t)$ in Fig. 2 is used in calculations. —: $\mathrm{Re}[y_{\text{TD-ANS}}(t)]$ in (16), ---: reference solution, ● ● ●: experimental-numerical results.

DOI: 10.1587/elex.13.20151041
Received December 7, 2015
Accepted December 28, 2015
Publicized January 18, 2016
Copyedited February 10, 2016

response waveform Re[$y_{\text{exp-num}}(t)$] (● ● ●: closed circles) obtained from the experimental-numerical results (see Section 2.2 and Fig. 3(b)), respectively. Please note that we modified the standard of the Re[$y_{\text{exp-num}}(t)$] to that of the Re[$y_{\text{reference}}(t)$] at the time $t = 2.81$ ns. As to a computational time, it takes 6 minutes 40 seconds for the Re[$y_{\text{reference}}(t)$] and approximately 1 second for the Re[$y_{\text{TD-ANS}}(t)$]. Therefore, the computation rate ratio of the TD-ANS to the reference solution is about 400. We can confirm the validity and practicality of the TD-ANS by comparing with the reference solution and the experimental-numerical results.

Next, we consider in detail an interpretation method of the response waveform Re[$y_{\text{reference}}(t)$] in Fig. 3(a) using the Re[$y_{\text{TD-ANS}}(t)$] in (16) associated with (17) and (18). Figs. 4(a) and 4(b) show propagation paths of pulse wave elements (❶~⓬). From the arrival time differences of the pulse wave elements, the Re[$y_{\text{reference}}(t)$] in Fig. 3(a) can be divided into 3 wave packets (i), (ii), and (iii). However, it is difficult to understand that the 3 wave packets are composed of these 12 pulse wave elements. In order to interpret the Re[$y_{\text{reference}}(t)$], we show in Fig. 3(c) the waveforms (—: solid curve) of pulse wave elements (❶~⓬). Please note that the pulse wave elements are indicated by the different scales. By comparing Fig. 3(a) with Fig. 3(c), we can observe that the wave packet (i) is attributed to the interference of the Re[$y_{\text{TD-RGO}}(t)$] in ❶ reflected on the convex surface (see Fig. 4(b)) and the Re[$y_{\text{A,RGO}_0}(t)$] in ❷ excited by the edge A (see

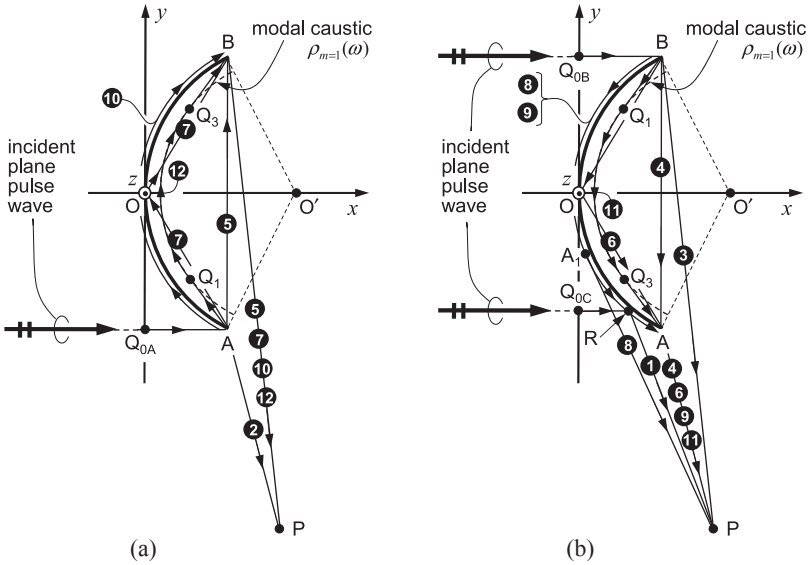

Fig. 4. Propagation phenomena of transient scattered field observed at the observation point $P(r, \psi) = (0.8\,\text{m}, 280°)$ (see Fig. 1(a)). (a) Propagation paths of transient scattered field elements excited by the edge A. ❷: $Q_{0A} \to A \to P$, ❺: $Q_{0A} \to A \to B \to P$, ❼: $Q_{0A} \to A \to O \to B \to P$, ❿: $Q_{0A} \to A \curvearrowright B \to P$, ⓬: $Q_{0A} \to A \to Q_1 \curvearrowright Q_3 \to B \to P$. (b) Propagation path of the transient RGO reflected on the convex surface and propagation paths of transient scattered field elements excited by the edge B. ❶: $Q_{0C} \to R \to P$, ❸: $Q_{0B} \to B \to P$, ❹: $Q_{0B} \to B \to A \to P$, ❻: $Q_{0B} \to B \to O \to A \to P$, ❽: $Q_{0B} \to B \curvearrowright A_1 \to P$, ❾: $Q_{0B} \to B \curvearrowright A \to P$, ⓫: $Q_{0B} \to B \to Q_1 \curvearrowright Q_3 \to A \to P$.

DOI: 10.1587/elex.13.20151041
Received December 7, 2015
Accepted December 28, 2015
Publicized January 18, 2016
Copyedited February 10, 2016

Fig. 4(a)). While we can see that the bundle of pulse (ii) is made up of 6 pulse wave elements, namely, the Re[$y_{B,RGO_0}(t)$] in ❸, the Re[$y_{B,RED_0}(t)$] in ❹, the Re[$y_{B,RED_1}(t)$] in ❻, the Re[$y_{B,SD_1}(t)$] in ❽, the Re[$y_{B,CW_1ED}(t)$] in ❾, and the Re[$y_{B,WG_1}(t)$] in ⓫ (see Fig. 4(b)). Similarly, the bundle of pulse (iii) is composed of 4 pulse wave elements i.e., the Re[$y_{A,RED_0}(t)$] in ❺, the Re[$y_{A,RED_1}(t)$] in ❼, the Re[$y_{A,CW_1ED}(t)$] in ❿, and the Re[$y_{A,WG_1}(t)$] in ⓬ (see Fig. 4(a)). We confirm that the Re[$y_{TD\text{-}ANS}(t)$] can extract and observe each pulse wave element from the Re[$y_{reference}(t)$] even when pulse wave elements overlap mutually at the observation point P.

From the above-mentioned discussions, we can conclude that the TD-ANS in (15) for the transient scattered field from a curved open sheet excited by a UWB pulse wave is a useful new reference solution on engineering applications.

4 Conclusion

We have developed the time-domain (TD) asymptotic-numerical solution (TD-ANS) for a two-dimensional transient scattered field from a cylindrically curved conducting open sheet excited by an ultra-wideband (UWB) pulse wave. By comparing with the reference solution and experimental-numerical results, we confirmed the validity of the TD-ANS. We showed that the proposed TD-ANS is a useful new reference solution on engineering applications, because it is highly accurate and is useful in understanding transient scattering phenomena, and its computation rate is very fast compared with that of the reference solution.

Acknowledgement

This work was supported in part by Japan Society for the Promotion of Science (JSPS) KAKENHI Grant Number 15K06094.

DOI: 10.1587/elex.13.20151041
Received December 7, 2015
Accepted December 28, 2015
Publicized January 18, 2016
Copyedited February 10, 2016